

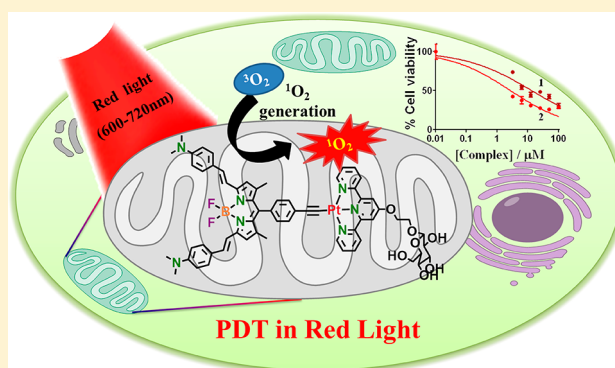
Glucose-Appended Platinum(II)-BODIPY Conjugates for Targeted Photodynamic Therapy in Red Light

Vanitha Ramu,[†] Srishti Gautam,[‡] Aditya Garai,[†] Paturu Kondaiah,^{*,‡} and Akhil R. Chakravarty^{*,†}

[†]Department of Inorganic and Physical Chemistry and [‡]Department of Molecular Reproduction, Development and Genetics, Indian Institute of Science, Bangalore 560012, India

Supporting Information

ABSTRACT: Platinum(II) complexes [Pt(L¹)(R-BODIPY)]Cl (1) and [Pt(L²)(R-BODIPY)]Cl (2), where R-BODIPY is 8-(4-ethynylphenyl)-distyryl-4,4-difluoro-5,7-dimethyl-4-bora-3a,4a-diaza-s-indacene-3, L¹ is 4'-phenyl-2,2':6',2''-terpyridine, and L² is (2,2':6',2''-terpyridin-4'-oxy)ethyl-β-D-glucopyranoside, were synthesized and characterized, and their photocytotoxicity was studied. The phenylacetylide complex [Pt(L¹)(C≡CPh)]Cl (3) was prepared and used as a control. Complexes 1 and 2 showed near-IR absorption bands at 713 nm ($\epsilon = 3.47 \times 10^4 \text{ M}^{-1} \text{ cm}^{-1}$) and 715 nm ($3.2 \times 10^4 \text{ M}^{-1} \text{ cm}^{-1}$) in 10% dimethyl sulfoxide (DMSO)–Dulbecco's Modified Eagle's Medium (DMEM) (pH 7.2). The BODIPY complexes are emissive in 10% DMSO–DMEM at pH 7.2 with $\lambda_{\text{em}} (\lambda_{\text{exc}} \Phi_f) = 822 \text{ nm} (710 \text{ nm}, 0.022)$ for complex 1 and $\lambda_{\text{em}} (\lambda_{\text{exc}} \Phi_f) = 825 \text{ nm} (710 \text{ nm}, 0.026)$ for complex 2. They generated singlet oxygen (¹O₂) in red light as evidenced from 1,3-diphenylisobenzofuran (DPBF) titration experiments. The singlet oxygen quantum yield (Φ_{Δ}) values for 1 and 2 were ~0.6 signifying their photosensitizing ability. They were remarkably photodynamic therapy (PDT) active in red light showing significant red light-induced cytotoxicity in cervical HeLa, lung cancer A549, and breast cancer MCF-7 cells (IC₅₀: 2.3–24.7 μM in light) with negligible dark toxicity (IC₅₀ > 100 μM). A significant enhancement in cellular uptake was observed for 2 having glucose-appended terpyridine ligand compared to 1. The confocal microscopy showed significant mitochondrial localization of the complexes as evidenced from the JC-1 assay. The complexes released the photoactive R-BODIPY ligand upon red light-irradiation as evidenced from the mass and ¹H NMR spectral studies. Complex 2 is remarkable in satisfying the essential requirements of targeted PDT in red light.



INTRODUCTION

Targeted chemotherapy has emerged as a viable alternative to chemotherapy to eliminate the drawbacks associated with the chemotherapeutic drugs such as cisplatin and its analogues, which lack specificity.^{1–3} To overcome these limitations, platinum(IV) prodrugs were designed as an alternative method to minimize the side effects of the platinum-based drugs, which have the ability to generate the active platinum(II) species either upon photoactivation or cellular reduction through a process of photoactivated chemotherapy (PACT).^{4–6} Photodynamic therapy (PDT) has developed as a viable photochemotherapeutic method, where a photosensitizer, namely, Photofrin as a drug is specifically activated inside the cancer cells under red light for the generation of reactive oxygen species (ROS) that damages the cancer cells without affecting the unexposed normal cells.^{7,8} In contrast to the conventional therapy, PDT enables selective drug action and improved drug specificity.^{9,10} Currently, platinum(II)-based PDT agents with photoimaging properties are studied to get insight about the drug distribution in vivo and for probable therapeutic use.^{11–13} In this context, near-infrared (NIR) light PDT agents are of particular importance, as NIR light within therapeutically relevant 700–850 nm region

possesses deep tissue penetration capability and can effectively eliminate tissue auto fluorescence interference. In addition, NIR light-based platinum compounds with photoimaging function could provide insights about cellular drug distribution.^{14–16}

By appending sugar, peptides, folic acid, etc. on the ligands of the desired complexes selective accumulation of drugs inside the tumor cells can be achieved, which would greatly enhance the targeting efficacy of an anticancer agent.^{17–19} A large variety of tumors have glucose transporter GLUT-1 overexpressed, and higher cellular uptake of the complexes into tumors can be ensured by appending a glucose moiety to the ligand, which provides targeting efficacy while increasing the drug aqueous solubility.^{20,21} In addition, directing the anticancer agent to mitochondrial DNA is likely to augment its anticancer potential by overcoming the resistance due to enhanced mitochondrial DNA (mtDNA) mutation and lack of nuclear excision repair (NER) machinery in the mitochondria of the cancer cells.^{22,23} There are reports of platinum(II) ring-fused chlorins and platinum(II) conjugates appended with macrocyclic PDT-based photosensitizers

Received: September 1, 2017

as near-IR PDT agents.²⁴ The recent reports have shown that combination therapy involving a platinum chemotherapeutic drug and a photosensitizer as a PDT agent increases the efficacy of the platinum drugs as antitumor agents by reducing the dark toxicity.^{25–27} 4,4-Difluoro-5,7-dimethyl-4-bora-3a,4a-diaza-s-indacene-3 (BODIPY) derivatives as photosensitizers are of interest for their excellent photophysical properties, and few of the BODIPY dyes are reported to predominantly localize in the mitochondria of the cancer cells.^{28,29} We recently reported Pt-BODIPY conjugates as mitochondria targeting PDT agents that are suitable for cellular imaging.^{30,31}

In the present work, we aimed to achieve two objectives by designing a new class of platinum(II) complexes, namely, $[\text{Pt}(\text{L}^1)(\text{R-BODIPY})]\text{Cl}$ (**1**), $[\text{Pt}(\text{L}^2)(\text{R-BODIPY})]\text{Cl}$ (**2**) (R-BODIPY = 8-(4-ethynylphenyl)-distyryl-BODIPY) having cancer cell targeting glucose moiety on the terpyridine (tpy) moiety (in L^2) for targeted chemotherapy and a photoactive BODIPY ligand (R-BODIPY) for generating singlet oxygen on activation with red light for PDT activity (Figure 1). Complex

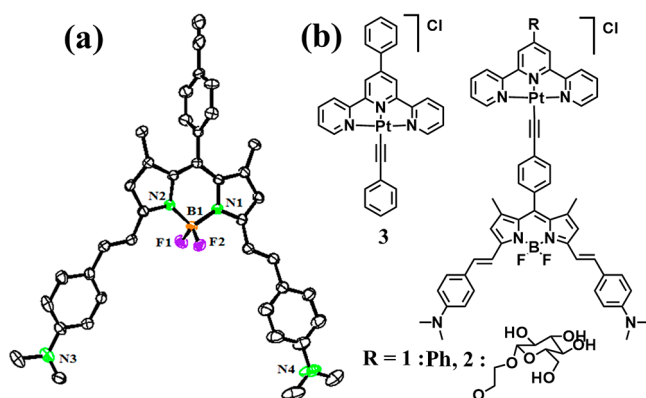


Figure 1. (a) Perspective view of the ligand R-BODIPY showing 50% probability thermal ellipsoids. Color codes: F purple, B orange, N green, H and C, black. H atoms other than the acetylenic proton are omitted for clarity. (b) Chemical structures of the platinum(II) complexes **1–3**.

$[\text{Pt}(\text{L}^1)(\text{phenylacetylide})]\text{Cl}$ (**3**) was used as a control. The complexes **1** and **2** are suitable for cellular imaging. The R-BODIPY ligand is incorporated in the structure of the complexes to achieve predominant localization in the mitochondria in preference to the nucleus. The addition of glucose moiety in L^2 is for higher cellular uptake of the complex besides increasing its aqueous solubility. The photolability of the $\text{Pt}^{\text{II}}-\text{C}\equiv\text{CR}$ bond enabled us to release the R-BODIPY ligand as a PDT agent on red light activation with the released monofunctional platinum(II) unit acting as a potential DNA intercalator.³² The cytotoxicity of the complexes and R-BODIPY ligand was studied by 3-(4,5-dimethylthiazol-2-yl)-2,5-diphenyltetrazolium bromide (MTT) assay and crystal violet (CV) assay, which showed noticeable photocytotoxicity upon red light photoirradiation ($\lambda = 600\text{--}720\text{ nm}$; 30 J cm^{-2}) with negligible dark toxicity. To determine the positive role of the glucose moiety in targeting the cancer cells over the normal cells in complex **2** over complex **1**, cellular uptake study in A549 and HPL1D normal cells under analogous experimental conditions was performed. Dichlorofluorescein diacetate (DCFDA) assay indicated ROS generation for both **1** and **2**. Co-localization experiments with mitochondria-specific dye MitoTracker Green (MTG) in A549 lung cancer cells by confocal laser scanning microscopy (CLSM)

showed that complexes **1** and **2** were localized significantly in the mitochondria of the cells. JC-1 assay in A549 cancer cells studied by CLSM indicated alterations in mitochondrial transmembrane potential ($\Delta\psi_m$).

EXPERIMENTAL SECTION

Materials and Methods. K_2PtCl_4 was obtained from Arora Matthey, India. 4',6-Diamidino-2-phenylindole (DAPI) and MitoTracker Green FM (MTG) were purchased from Invitrogen. From S. D. Fine Chemicals and Sigma-Aldrich all other chemicals and reagents were purchased. Ligands and complexes were synthesized by following previous reports.^{32–34} ^1H NMR spectra were recorded by using a Bruker Avance 400 MHz NMR spectrometer. To obtain the mass spectral data Agilent 6538 Ultra High Definition Accurate Mass-Q-TOF (LC-HRMS) instrument was used. Elemental analysis was done with a Thermo Finnigan Flash EA 1112 CHNS analyzer. UV–visible, IR, and emission spectra were recorded with Bruker Alpha and PerkinElmer Spectrum 750 spectrophotometers and HORIBA Jobin Yvon IBH TCSPC fluorimeter (fitted with FluoroHub software analysis). The geometries of the complexes were optimized using basis sets B3LYP/LANL2DZ level of theory calculations.³⁵ A red light photo-reactor, namely, Waldmann PDT 1200 L, was used for all the experiments that required photoirradiation using standard protocols. Cytotoxic data by MTT and CV assay were obtained with a TECAN microplate reader and GraphPad Prism 7 software. Flow cytometric experiments were performed by using Becton Dickinson fluorescent activated cell sorting (BD-FACS) Verse instrument (BD Biosciences) configured with a MoFlo XDP cell sorter and analyzer with three lasers ($\lambda = 488, 365, \text{ and } 640\text{ nm}$) and 10-color parameters. Windows 7 operating system with BD-FACS suite software for acquisition and analysis was used for FACS analysis. Inductively coupled plasma mass spectroscopy (ICP-MS) method was employed to evaluate the cellular platinum content Thermo X series II. Zeiss LSM 880 with Airyscan confocal microscope was used to acquire confocal microscopy images using an oil immersion lens with magnification of 63 \times , and Zeiss software was used for processing of images.

Synthesis. Synthetic steps employed for the preparation of the R-BODIPY and the complexes are given in Schemes S1 and S2 (Supporting Information). Ligands L^1 , L^2 , the precursor complexes, namely, $[\text{Pt}(\text{L}^1)\text{Cl}]\text{Cl}$ (P^1) and $[\text{Pt}(\text{L}^2)\text{Cl}]\text{Cl}$ (P^2), and the phenylacetylide control complex (**3**) were synthesized and characterized using reported methods (Figures S1–S3, Supporting Information).^{36–38} The synthetic method for the complexes and the characterization data are given below.

$[\text{Pt}(\text{L})(\text{R-BODIPY})]\text{Cl}$ (**1**, **2**). The monofunctional platinum(II) complexes were synthesized by following literature procedures.^{34,36} R-BODIPY (200 mg, 0.33 mmol) ligand in anhydrous DMF (4 mL) was initially treated with freshly distilled triethylamine (TEA, 5 mL) for 1 h under nitrogen atmosphere. A solution of the respective precursor complex P^1 (94 mg, 0.165 mmol) for complex **1** or P^2 (118 mg, 0.165 mmol) for complex **2** was added in anhydrous dimethylformamide (DMF; 8 mL) along with CuI (10 mol %, catalytic amount). The resulting mixture was stirred under nitrogen for 72 h in dark and then concentrated using reduced pressure by using rotavac evaporator. A 2 mL aliquot of DMF was added to redissolve the residue, and excess of diethyl ether (60 mL) was added to precipitate the desired compound as solid. The product was isolated, washed twice with 50 mL of diethyl ether, vacuum-dried, and kept in the dark.

$[\text{Pt}(\text{L}^1)(\text{R-BODIPY})]\text{Cl}$ (**1**). Greenish-black solid. Yield: 54%. Anal. Calcd for $\text{C}_{60}\text{H}_{51}\text{BClF}_2\text{N}_7\text{Pt}$ (M_w : 1148.3603): C, 62.70; H, 4.47; N, 8.53. Found: C, 62.89; H, 4.50; N, 8.65%. ESI-MS m/z : Calcd $[\text{M}-\text{Cl}]^+$, 1113.3903. Found: 1113.3238. ^1H NMR (400 MHz, deuterated dimethyl sulfoxide ($\text{DMSO}-d_6$)): δ (ppm) 8.98 (s, 2 H), 8.87 (d, 6 H, $J = 6.5\text{ Hz}$), 8.51 (d, 4 H, $J = 7.6\text{ Hz}$), 8.20 (d, 4 H, $J = 3.2\text{ Hz}$), 7.92 (t, 5 H, $J = 6.5\text{ Hz}$), 7.68 (d, 6 H, $J = 3.2\text{ Hz}$), 7.45 (d, 2 H, $J = 16\text{ Hz}$), 7.24 (d, 2 H, $J = 16\text{ Hz}$), 6.79 (s, 1 H), 6.77 (s, 1 H), 3.04 (s, 12 H), 1.41 (s, 6 H). IR data (cm^{-1}): 3300 (br, w), 2920 (br, w), 2352 (w), 1600 (s), 1540 (s), 1410 (s), 1350 (sh), 1220 (s), 762 (m), 536 (w) (br, broad; w, weak; sh, shoulder; s, strong). UV–visible (10% dimethyl

sulfoxide (DMSO)–Dulbecco's Modified Eagle's Medium (DMEM) at pH 7.2): λ_{max} nm (ϵ , $\text{M}^{-1} \text{cm}^{-1}$) = 713 (34 700), sh 654 (27 400), 512 (11 900), 407 (20 700), 338 (35 200), 265 (35 000). Emission spectral data (10% DMSO–Dulbecco's phosphate-buffered saline (DPBS) at pH 7.2): λ_{em} (λ_{ex} , Φ_{f}) = 822 nm (710 nm, 0.022).

[Pt(L²)(R-BODIPY)]Cl (2). Greenish-black solid. Yield: 46%. Anal. Calcd for C₆₂H₆₁BClF₂N₇O₇Pt (M_w : 1295.5528): C, 57.48; H, 4.75; N, 7.57. Found: C, 57.30; H, 4.69; N, 7.61%. ESI-MS m/z : Calcd [(M-Cl)⁺-H+K]⁺, 1297.3176; Found, 1297.3176. ¹H NMR (400 MHz, DMSO-*d*₆): δ (ppm) 8.86 (s, 4 H), 8.68 (s, 4 H), 8.51 (s, 4 H), 8.32 (s, 4 H), 7.93 (s, 4 H), 7.45 (s, 4 H), 7.29 (s, 2 H), 6.88 (s, 2 H), 6.79 (s, 2 H), 5.16 (s, 1 H), 5.1 (s, 1 H), 5.03 (s, 1 H), 4.98 (s, 1 H), 4.58 (s, 3 H), 4.43 (s, 2 H), 4.31 (s, 1 H), 4.21 (s, 1 H), 3.85 (s, 2 H), 3.04 (s, 6 H), 2.99 (s, 3 H), 2.89 (s, 3 H), 1.17 (s, 6 H). IR data (cm^{-1}): 3300 (br, s), 1610 (s), 1475 (sh), 1421 (s), 1340 (sh), 1210 (s), 1168 (sh), 780 (m), 600 (w). UV/Visible (10% DMSO–DMEM at pH 7.2): λ_{max} nm (ϵ , $\text{M}^{-1} \text{cm}^{-1}$) = 715 (32 000), sh 651 (19 500), 512 (9500), 436 (18 500), 300 (64 000). Emission spectral data (10% DMSO–DPBS at pH 7.2): λ_{em} (λ_{ex} , Φ_{f}) = 825 nm (710 nm, 0.026).

X-ray Crystallographic Procedure. The crystal structure of ligand R-BODIPY was obtained by single-crystal X-ray diffraction method. The deep green colored rectangular block crystals of R-BODIPY were obtained on slow evaporation from a mixture of CH₂Cl₂ and methanol. The crystal was mounted on loop with paratone oil. All the intensity and geometric data were collected at 5 s frame⁻¹ scan rate by an automated Bruker SMART APEX CCD diffractometer fitted with a fine focus 1.75 kW sealed-tube Mo K α X-ray source (λ = 0.710 73 Å) with increasing ω (width of 0.3° per frame). Intensity data were collected with ω -2 θ scan mode and then corrected for Lorentz polarization and absorption effects.³⁹ WinGx suite of programs (version 1.63.04a) and SHELXL-2013 were used to solve the structure and for refinement.³⁹ The non-hydrogen atoms were refined with anisotropic displacement coefficients, and their coordinates were permitted to ride on their respective carbon atoms. Final refinement was performed by including atomic positions of all the atoms, anisotropic thermal parameters for all the non-hydrogen atoms, and isotropic thermal parameters for all the hydrogen atoms. ORTEP was used to obtain the perspective view.³⁹ Selected crystallographic parameters, bond distances, and angles are provided in Tables S1 and S2 (Supporting Information). The CCDC deposition number is 1563252.

Cellular Experiments. The CV assay and MTT assays were used for the determination of photocytotoxicity of the complexes in human cervical cancer (HeLa), human lung adenocarcinoma cell line (A549), human breast adenocarcinoma cell line (MCF-7), and immortalized human lung epithelial cell line (HPL1D) following the reported procedures.⁴⁰ The cell lines HeLa, A549, and MCF-7 cancer cell lines were preferentially selected, as these cell lines were reported to have overexpression of GLUT-1 glucose transporter.⁴¹ Cells were incubated at several concentrations of 1–3 from 0.718 to 100 μM in 1% DMSO–DMEM in the dark for 4 h. By replacing DMEM buffer with DPBS one of the sets of cells was exposed to red light for 40 min (λ = 600–720 nm; 30 J cm^{-2}) using Waldmann PDT 1200 L photoreactor keeping the other set of cells in dark. Data were obtained employing standard protocols with three independent sets of experiments performed in triplicate for each concentration. Cytotoxicity of the complexes in terms of IC₅₀ values was determined by nonlinear regression analysis (Graph Pad Prism 6). Confocal microscopy experiment was done for the intracellular localization of fluorescent complexes 1 and 2 (10 μM) in 1% DMSO–DMEM in A549 cells (Zeiss LSM 880 with Airyscan) with an oil immersion lens having a magnification of 63X. Mitotracker Deep Green and DAPI were used for cellular localization study as mitochondria and nucleus selective trackers, respectively. To ascertain the results, confocal microscopy experiments were performed in duplicate, and multiple CLSM images were analyzed. Cellular ROS was detected by DCFDA assay in A549 and HPL1D cells. Cellular uptake of the fluorescent complexes 1 and 2 was studied in A549 and HPL1D cells by FACS analysis. The cellular platinum content in complexes 1- and 2-treated A549 cells was measured by ICP-MS. The effect of the complexes on mitochondrial transmembrane potential ($\Delta\psi_m$) in A549 cells was measured by JC-1 assay.

RESULTS AND DISCUSSION

Synthesis and General Aspects. The ligand R-BODIPY and the complexes [Pt(L¹)(R-BODIPY)]Cl (1) and [Pt(L²)(R-BODIPY)]Cl (2) were synthesized in moderate yields and characterized from their physicochemical data (Figure 1 and Table 1). The corresponding phenylacetylide complex [Pt(L¹)-

Table 1. Selected Physicochemical Data for R-BODIPY, Complexes 1 and 2

	complex 1	complex 2	R-BODIPY
$\Lambda_m^a / \text{S m}^2 \text{M}^{-1}$	79	82	
UV-vis: ^b $\lambda_{\text{max}} / \text{nm}$ ($1 \times 10^{-4} \epsilon / \text{M}^{-1} \text{cm}^{-1}$)	713 (3.5), sh 654 (2.7), 512 (1.2)	715 (3.2), sh 651 (1.95), 512 (0.95)	720 (4.4), sh 656 (1.9), 514 (1.3)
emission: ^b $\lambda_{\text{em}} / \text{nm}$ (Φ_{f})	822 (0.022)	825 (0.026)	826 (0.18) ^c
¹ O ₂ quantum yield ^d (Φ_{Δ})	0.57	0.58	
¹ H NMR δ (ppm) of β -protons ^e	6.77, 6.79	6.79, 6.88	6.69, 6.72

^aMolar conductivity in DMF. ^bIn 10% DMSO–DMEM solution. ^c Φ_{f} of RBODIPY from ref 33. ^dIn DMSO with Rose Bengal as standard (Φ_{Δ} : 0.76). ^eChemical shift of β -protons of BODIPY in DMSO-*d*₆.

(C \equiv CPh)]Cl (3) was prepared and used as a control. The ¹H NMR spectral and elemental analysis data ascertained the purity of the complexes. Complexes 1 and 2 showed respective mass spectral (HR-MS) peaks in methanol at 1113.3238 and 1297.3176 assignable to [M-Cl]⁺ and [(M-Cl)+K-H]⁺ along with isotopic distribution of platinum in the peaks (Figures S4 and S5, Supporting Information). The ¹H NMR spectra of 1 and 2 showed the characteristic signals corresponding to the tpy, R-BODIPY, and glucose moieties; the disappearance of acetylenic proton of R-BODIPY and the shift in proton signals of R-BODIPY on complexation suggest the formation of the complexes (Figures S6–S10, Supporting Information). The ¹³C NMR signals of the complexes could not be observed, despite a prolonged acquisition time, due to insufficient solubility of the complexes. The IR spectra of both the complexes showed two intense peaks within 1620–1590 cm^{-1} and 1540–1475 cm^{-1} due to respective C=N and conjugated C=C of pyrrole ring stretching frequencies corresponding to R-BODIPY (Figure S11, Supporting Information). Complex 2 showed an intense broad peak at 3300 cm^{-1} corresponding to OH group stretching due to the presence of the glucose moiety. The molar conductivity values of $\sim 82 \text{ S m}^2 \text{M}^{-1}$ in DMF at 25 °C suggest 1:1 electrolytic nature of the complexes (Table 1). The solubility of the complexes was moderate in common organic solvents. The solution stability of the complexes at pH 7.2 was determined in the dark and light (400–700 nm) in 10% DMSO–DMEM solution by UV–visible measurements up to 48 h (Figure S12, Supporting Information).

Electronic Spectroscopy. The UV–visible spectra of the complexes recorded in 10% DMSO–DMEM at pH 7.2 showed strong absorption bands corresponding to the electronic transitions relating to the R-BODIPY and terpyridine moieties in the ranges of 713–715 nm and 250–350 nm, respectively (Figure 2a).^{42,43} Both the complexes have lowest-energy absorption in the red region due to the dimethylamino donor groups as chromophore in styryl substituents in R-BODIPY.^{43a} In addition, both complexes 1 and 2 showed shoulder peaks at 654 and 651 nm, respectively. The bands in the 250–350 nm range are due to the contribution of the intraligand (IL) $\pi \rightarrow \pi^*$ transitions of the tpy and alkynyl ligands, particularly noticeable for complex

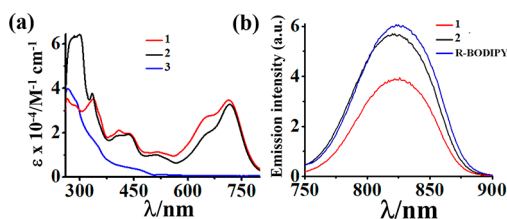


Figure 2. (a) The electronic absorption spectra of the complexes 1–3 and (b) emission spectra ($\lambda_{\text{ex}} = 710 \text{ nm}$) of R-BODIPY, complexes 1 and 2 in 10% DMSO–DMEM at pH 7.2.

2 in comparison to 1.⁴² The complexes 1 and 2 displayed broad fluorescence emission spectra with emission maximum at 822 and 825 nm on exciting with $\lambda_{\text{ex}} = 710 \text{ nm}$ similar to the emission of R-BODIPY (Figure 2b). There is a noticeable Stoke shift in the emission spectra of both the complexes due to partial charge transfer character of the emission of the dimethylamino-containing species.^{33,43} Both the complexes showed BODIPY-based fluorescence quantum yields with Φ_{F} value of 0.022 for complex 1 and 0.026 for complex 2 that are significantly lower compared to R-BODIPY with the reported Φ_{F} value of 0.18.³³ The lower fluorescence quantum yield of the complexes provides an indirect evidence of having better photosensitizing ability in platinum(II) bound form in comparison to only R-BODIPY ligand.⁴⁴

Energy-Minimized Structure from Density Functional Theory. The quantum calculation analysis was used to optimize the structures of the complexes by employing B3LYP/LANL2DZ level of theory for all the atoms (Figure 3, Table S3, and Figures S13 and S14, Supporting Information).³⁵ Frontier orbitals were mapped on the atoms from the electronic charge density distribution. The highest occupied molecular orbital (HOMO) for the complexes 1 and 2 is localized on the R-BODIPY moiety, while the lowest unoccupied molecular orbital (LUMO) is primarily localized on the terpyridine-Pt core. The dipole-allowed transitions for the complexes are registered in Table S4, Supporting Information. The structures exhibited a strongly favored

transition band at 682 nm with oscillator strength of 0.85 for complex 1 and at 659 nm with oscillator strength of 0.68 for complex 2. These visible region bands are due to the transitions that are from MOs localized on R-BODIPY moiety to MOs localized on R-BODIPY moiety in both the complexes.

Single-Crystal X-ray Crystallography. The solid-state structure of the R-BODIPY ligand was determined by single-crystal X-ray diffraction method. The ligand R-BODIPY crystallized in $P\bar{1}$ space group (No. 2) with $Z = 2$ (Figure 1a). The $\text{C}\equiv\text{C}$ bond distance was found to be 1.018(5) Å. The bond lengths of B(1)–F(1) and B(1)–F(2) are 1.389(4) and 1.389(4) Å, respectively. The N(1)–B(1) and N(2)–B(1) bonds are of 1.544(4) and 1.540(4). The F(1)–B(1)–F(2), N(1)–B(1)–N(2), and N(2)–B(1)–N(1) angles are 108.4(3)°, 110.8(3)°, and 107.0(2)°, respectively. The bond lengths and angles compare well to the reported crystal structure of the precursor of R-BODIPY having iodine atom instead of $\text{C}\equiv\text{C}$ bond, which also crystallizes in the same space group $P\bar{1}$.⁴⁵ The

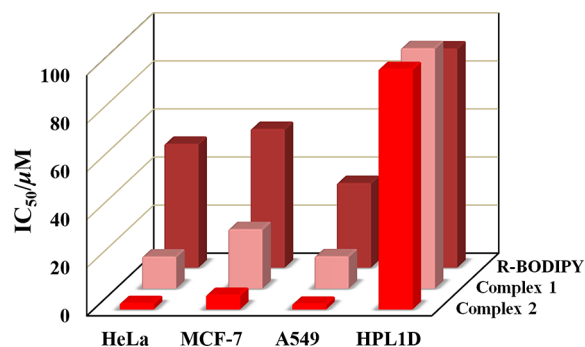


Figure 4. Photocytotoxicity from MTT assay of R-BODIPY (brown bars), complexes 1 (light pink bars), and 2 (red bars), in HeLa, MCF-7, A549, and HPL1D cells after 4 h of incubation in dark followed by red light irradiation ($\lambda = 600\text{--}720 \text{ nm}$; 30 J cm^{-2}). IC₅₀ values are greater than 90 μM in dark. Errors are within $\pm 5\%$.

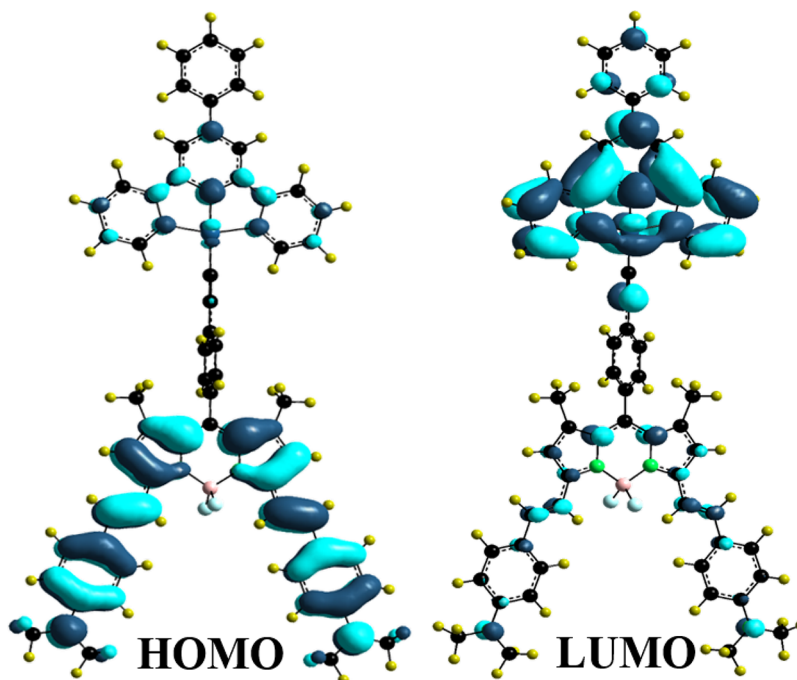


Figure 3. Frontier molecular orbitals, namely, HOMO and LUMO of complex 1 as obtained by density functional theory using B3LYP/LanL2DZ level of theory.

Table 2. MTT and Crystal Violet Assay Data ($IC_{50}/\mu M$) of Complexes 1, 2, and R-BODIPY Ligand

cell	complex 1		complex 2		R-BODIPY	
	MTT	CV	MTT	CV	MTT	CV
HeLa L ^a	13.3 ± 0.2	17.7 ± 0.1	2.6 ± 0.2	5.5 ± 0.1	51.5 ± 0.1	67.7 ± 0.4
D ^b	>100	>100	91.4 ± 0.2	>100	>100	>100
MCF-7 L ^a	24.7 ± 0.2	55.2 ± 0.2	6.0 ± 0.4	14.4 ± 0.1	57.7 ± 0.1	81.4 ± 0.2
D ^b	>100	>100	>100	>100	>100	>100
A549 L ^a	13.4 ± 0.1	28.8 ± 0.2	2.3 ± 0.1	7.8 ± 0.2	35.2 ± 0.2	62.5 ± 0.1
D ^b	>100	>100	>100	>100	>100	>100
HPL1D L ^a	>100	>100	>100	>100	91.2 ± 0.1	>100
D ^b	>100	>100	>100	>100	>100	>100

^a IC_{50} values (μM) were for 4 h preincubated in the dark followed by 40 min of exposure to visible light (L, 600–720 nm; 30 J cm⁻²; Waldmann PDT 1200 L) and post incubation of 19 h in dark. ^bIn dark (D) with 4 h preincubation time followed by 20 h of post incubation.

unit-cell packing diagram of R-BODIPY and selected bond distances and angles are given as Supporting Information (Figure S15 and Tables S1 and S2, Supporting Information).

Cell Viability Studies. The photoinduced antitumor activity of the platinum complexes 1 and 2 along with R-BODIPY was investigated on HeLa, MCF-7, A549, and HPL1D cells in dark and light (red light, $\lambda = 600\text{--}720$ nm, 30 J cm⁻²) by MTT assay (Figure 4 and Table 2). In this assay, the dark purple formazan crystals that are insoluble in DMEM but soluble in DMSO, which are formed due to the cleavage of tetrazolium rings of MTT by mitochondrial dehydrogenases of viable cells, can be quantified from spectral measurements. The half maximal inhibitory concentrations (IC_{50}) for complex 2 were within 2.3 to 6.0 μM and for complex 1 within 13.3 to 24.7 μM in HeLa, A549, and MCF7 cells upon red light photoirradiation ($\lambda = 600\text{--}720$ nm; 30 J cm⁻²), respectively (Figure 4, Table 2, and Figures S16–S18, Supporting Information). The half maximal inhibitory concentration (IC_{50}) for complex 3 was above 100 μM in all the cell lines studied both upon red light photoirradiation ($\lambda = 600\text{--}720$ nm, 30 J cm⁻²) and dark. The MTT assay data reveal that both the complexes 1 and 2 are significantly photocytotoxic in red light, while being less toxic in the dark. The higher activity of 2 than 1 is due to the appended glucose moiety on the terpyridine ligand, which enhances the cellular uptake of 2 compared to 1.

To validate that the MTT assay is a true reflection of the cytotoxicity by the complexes, we performed CV assay in these cells in dark and light ($\lambda = 600\text{--}720$ nm, 30 J cm⁻²). CV assay is one of the direct methods that measure the DNA mass of living cells. The metabolism-independent CV assay involves a triaryl-methane dye that has affinity to the exterior part of the DNA, and the quantity of dye absorbed is related to the viable cells total DNA content.⁴⁶ The half maximal inhibitory concentrations (IC_{50}) for complex 2 was within 5.5 to 14.4 μM and for complex 1 within 17.7 to 55.2 μM in HeLa, A549, and MCF7 cells upon red light photoirradiation ($\lambda = 600\text{--}720$ nm; 30 J cm⁻²) with IC_{50} value of >100 in dark (Table 2 and Figures S19–S22, Supporting Information). The lower IC_{50} values obtained for MTT assay can be accounted to disrupted MTT tetrazolium salt reduction rate by the complexes 1 and 2. These complexes

localize to mitochondria and influence its function. However, CV staining data also suggest that both the complexes are significantly photocytotoxic in red light, with nominal dark toxicity and higher activity of 2 than 1 as evidenced from the MTT assay.

Cellular Uptake. Flow cytometry was performed for the determination of cellular uptake property of the complexes. Both MTT and CV assay data showed higher cytotoxicity of complex 2

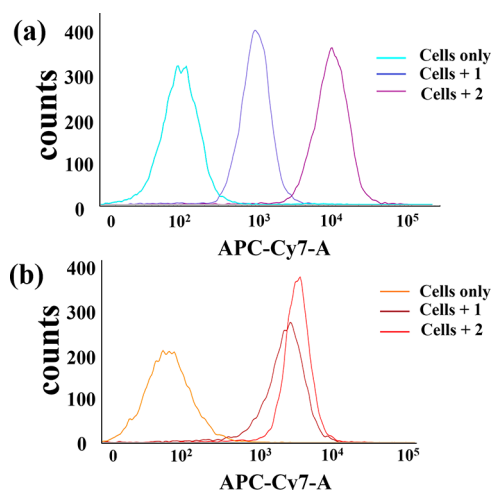


Figure 5. Quantitative analysis of cellular uptake of the complexes by flow cytometry upon incubating A549 cells (a) and HPL1D (b) with complexes 1 and 2 (15 μM) at 37 °C for 4 h with cells untreated used as a control. The observed shift in the band position of complexes 1 and 2 in A549 cells clearly indicates that 2 has higher cellular uptake over 1. The minor shift in HPL1D cells clearly suggests that complexes 1 and 2 have similar cellular uptake in the normal cells.

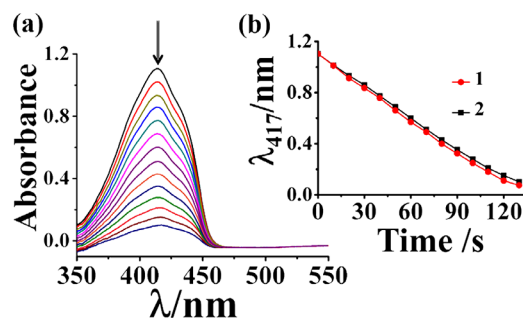


Figure 6. (a) Spectral changes of DPBF with time at 417 nm treated with complex 2 in DMF. (b) The linear plot showing a gradual decrease in absorbance of DPBF at 417 nm with time on light exposure of the complexes 1 (red line) and 2 (black line) at 5 s intervals. Both complexes showed similar extent of ¹O₂ generation.

Table 3. Cellular Uptake Data of the Complexes 1 and 2

complex	platinum content ^a (ng per 1 × 10 ⁵ cells)
1	7.6 ± 0.4
2	24.5 ± 0.6

^aA549 cells treated with the complexes (10 μM) for 4 h in the dark. The platinum content estimated by the ICP-MS method.

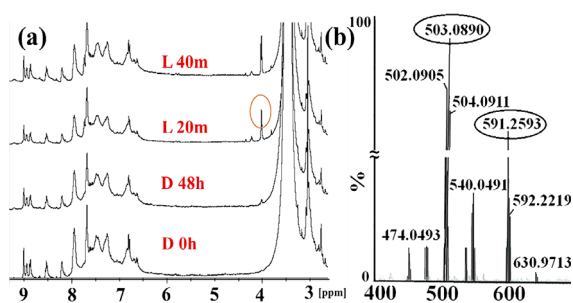


Figure 7. (a) ^1H NMR spectral changes of complex **1** in $\text{DMSO-}d_6$ in dark (D) at different time intervals and in light (L, 600–720 nm) of different photoexposure time. (b) Mass spectrum of **1** on red light exposure ($\lambda = 600\text{--}720\text{ nm}$; 30 J cm^{-2}). Peaks at 503 and 591 (m/z) are for $[(\text{L}^1)\text{Pt-H}]^+$ fragment and $[\text{M-F}]^+$ of R-BODIPY, respectively.

than **1**. Appendage of a glucose moiety to the terpyridine ligand at C-1 position of glucose is likely to enhance the cellular uptake of **2**, and this was observed from this study.⁴⁷ Relevant data are given in Table 3. Nearly 100% of cells treated with complexes showed increased fluorescence in A549 lung cancer cells and HPL1D normal cells by FACS analysis. Compared to **1**, A549 cells treated with complex **2** after 4 h of incubation showed remarkably high fluorescence intensity at 5, 10, and 15 μM suggesting high cellular uptake of **2** (Figure 5a and Figures S23 and S24, Supporting Information). Cellular uptake was lower in HPL1D normal cells under analogous experimental conditions implying the positive role of the glucose moiety in targeting the cancer cells over normal cells (Figure 5b). The quantification of

cellular platinum enabled us to observe higher cellular uptake of complex **2** compared to complex **1** by ICP-MS in A549 cells. The cells incubated with the complex at 10 μM for 4 h were digested to form sample solution following the standard protocols. As can be seen from Table 3, the platinum content in complex **2**-incubated cells was determined as $\sim 24.5\text{ ng}$ per 1.0×10^5 cells, while the metal content in complex **1**-incubated cells was determined as $\sim 7.6\text{ ng}$ per 1.0×10^5 cells. The Pt content got significantly enhanced in complex **2** than **1** displaying an approximately threefold enhancement factor.

Cellular ROS Generation. The quantification of photoinduced cellular generation of ROS being of importance in PDT, DCFDA assay was performed in A549 cancer cells and HPL1D normal cells by recording the green fluorescence of 2',7'-dichlorodihydrofluorescein (2,7-DCF) ($\lambda_{\text{em}} = 525\text{ nm}$, $\lambda_{\text{ex}} = 488\text{ nm}$). Cellular ROS oxidize cell-permeable DCFDA generating a fluorescent 2,7-DCF having emission maxima at 528 nm. Flow cytometry analysis was done to determine the percentage population of cells generating ROS. To account for the lower cytotoxicity of the complexes in HPL1D normal cells compared to A549 cancer cells, DCFDA assay in both A549 cells and HPL1D cells was performed at their IC_{50} values (**1**: 10 μM and **2**: 2.5 μM for A549 cells and **1**: 100 μM and **2**: 100 μM for HPL1D cells) followed by 4 h of postincubation and red-light photoirradiation ($\lambda = 600\text{--}720\text{ nm}$; 30 J cm^{-2}). By FACS the distribution of DCFDA-stained A549 cells and HPL1D cells was obtained in the FL-1 channel. For both A549 cells and HPL1D cells treated with the complexes after photoirradiation, there was a significant shift observed in the fluorescence bands

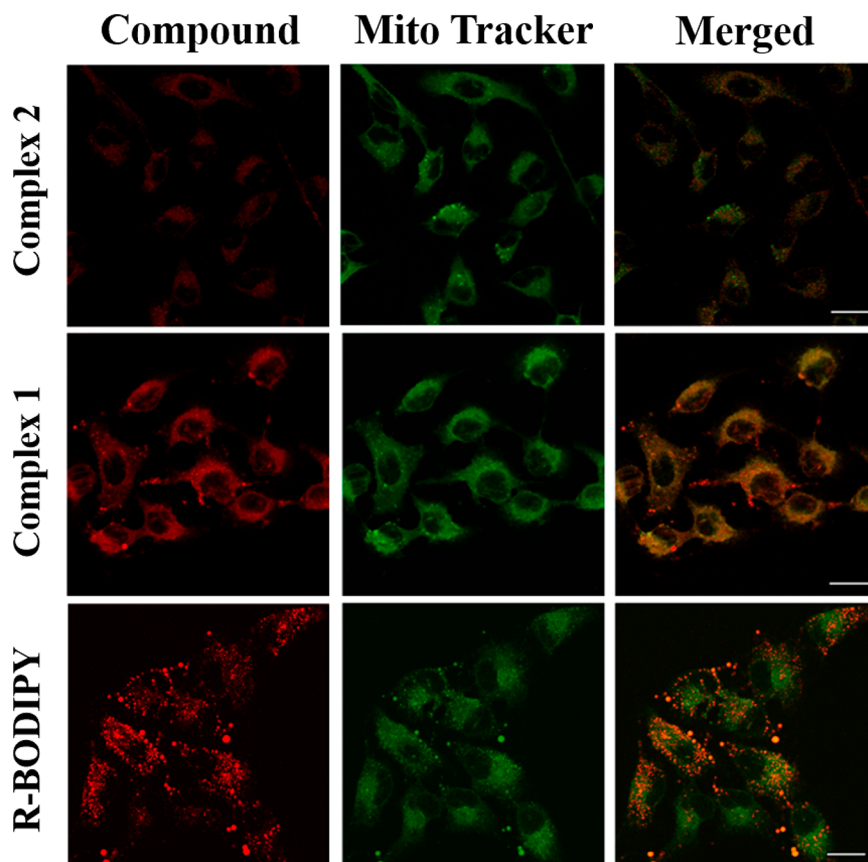


Figure 8. Confocal microscopic images of A549 cells incubated with R-BODIPY (20 μM), complexes **1** and **2** (10 μM) for 4 h at 37 $^{\circ}\text{C}$. Cells were viewed in the green channel for MTG and the red channel for R-BODIPY, complexes **1** and **2**. The yellow areas in the merged panels indicate significant colocalization of the compounds within mitochondrial compartments. Scale bar is 20 μm in all the panels.

compared to the only DCFDA dye-treated cells or the complex-treated cells kept in dark. The shifts indicated the generation of ROS in both A549 and HPL1D cells but at lower concentrations in A549 compared to HPL1D (Figures S25–S27, Supporting Information).

Singlet Oxygen Quantum Yield. One of the objectives of coordinating R-BODIPY unit with platinum is to photogenerate singlet oxygen species as the ROS for which there is no apparent defense mechanism existing in the cellular system. The singlet oxygen generation was studied from an experiment using 1,3-diphenyl isobenzofuran (DPBF; 20 μM) as a $^1\text{O}_2$ scavenger treated with both the complexes **1** and **2** (5 μM ; Figure 6). The absorption spectra of DPBF were recorded after each photoirradiation for 5 s ($\lambda = 600\text{--}720$ nm; 30 J cm^{-2}). The linear plots of similar slopes indicate the gradual decrease in intensity of the band at 417 nm suggesting singlet oxygen as the ROS with nearly equal efficacy for both complexes (Figure 6b). The singlet oxygen quantum yield of the complexes was measured using Rose Bengal as a standard. The values are 0.57 for complex **1** and 0.58 for complex **2**.⁴⁸

Photo Release of R-BODIPY. We recently reported that platinum(II) acetylenic bond Pt–C \equiv CR in the conjugates can be cleaved on photoirradiation.³⁷ This led us to study the spectral changes associated with complexes **1** and **2** upon red light irradiation. The ^1H NMR spectra of complex **1** in DMSO- d_6 were monitored on exposure to red light ($\lambda = 600\text{--}720$ nm; 30 J cm^{-2}). The spectral traces are shown in Figure 7a. A new peak was found to appear at 4.01 ppm after 20 min of photoirradiation. This peak is assignable to an acetylenic proton of

the released R-BODIPY ligand.^{34,37,49} The complex showed its solution stability in dark even after 48 h as demonstrated from the ^1H NMR spectral study (Figure 7a). This suggests that the spectral changes observed are due to photoirradiation of the complex. The mass spectra of the irradiated sample recorded after 40 min of photoirradiation showed two major peaks at 591.2593 corresponding to [M-F] $^+$ of the R-BODIPY moiety and at 503.0890 corresponding to the [(L 1)Pt–H] $^+$ unit (Figure 7b and Figure S28, Supporting Information) suggesting the cleavage of the platinum(II)–carbon bond in Pt–C \equiv CR.³⁷

Cellular Localization. Selective localization and cell targeting being of paramount importance in targeted PDT, we performed the colocalization experiments with mitochondria-specific dye MTG in A549 cancer cells by CLSM. The cells were treated with the fluorescent complexes **1** (10 μM) and **2** (10 μM) and R-BODIPY (20 μM) at 37 $^\circ\text{C}$ for 4 h. Complex **2** showed significantly higher fluorescence intensity than **1** due to its enhanced cellular uptake (Figure 8). The merged CLSM images showed that R-BODIPY and the complexes were localized significantly in the mitochondria of the cells giving Pearson's coefficient value measured for R-BODIPY as 0.77 and complex **2** as 0.72 (Figure S29, Supporting Information).⁵⁰ Pearson's coefficient value of complex **1** could not be obtained due to lower fluorescent signals. DAPI was used for selective nuclear staining, and the CLSM images showed no apparent localization of the complexes in the cell nucleus (Figure S30, Supporting Information).

Mitochondrial Membrane Potential. The generation of ROS triggered by the complexes localized in mitochondria in

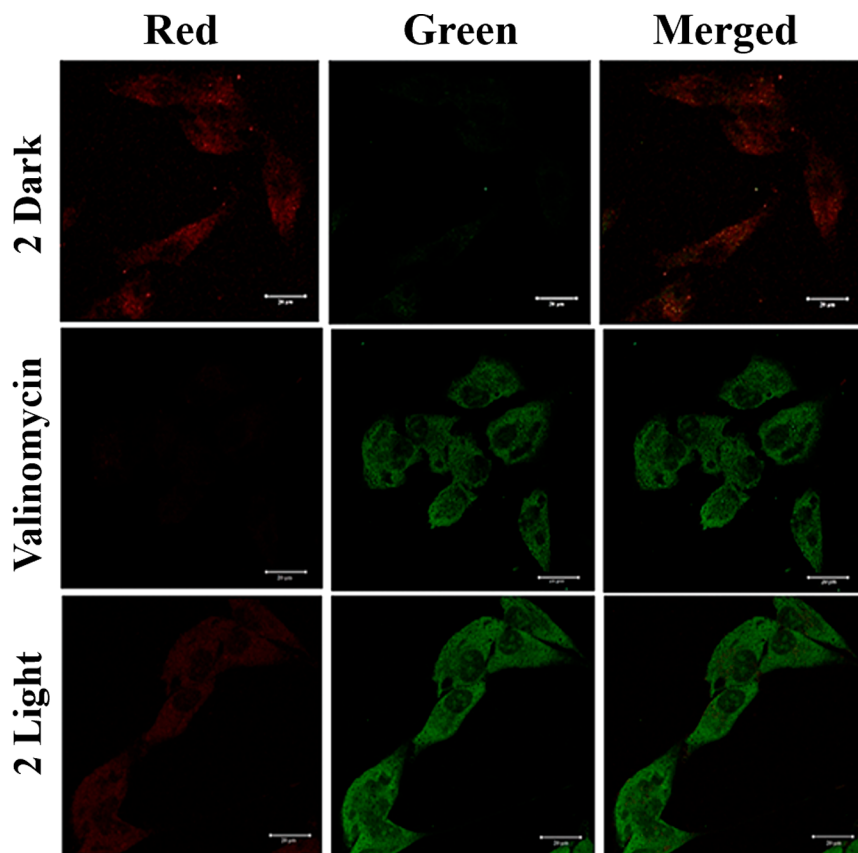


Figure 9. Confocal microscopic images of JC-1 assay showing the fluorescence images of JC-1 dye in both red and green channel in A549 cells incubated with complex **2** (10 μM) for 4 h at 37 $^\circ\text{C}$ for dark and on red light photoirradiation ($\lambda = 600\text{--}720$ nm; 30 J cm^{-2}) for light. The last column shows merged images of green and red channel. Scale bar is 20 μm in all the panels.

the presence of red light could lead to variations in mitochondrial transmembrane potential $\Delta\psi_m$. The cell-permeant 5,5',6,6'-tetrachloro-1,1',3,3'-tetraethylbenzimidazolylcarbocyanine iodide (JC-1 dye) has potential dependent dual emissive property and is employed as a probe to determine changes occurring in mitochondrial potential. Inside the mitochondria, JC1 dye forms red fluorescent J-aggregates ($\lambda_{em} = 590$ nm), and a decrease in $\Delta\psi_m$ leads to leakage of JC-1 dye into cytosol, where it occurs as a monomer that emits green fluorescence ($\lambda_{em} = 530$ nm). A549 cells treated with complex **2** (2.5 μ M) on red light irradiation diminished the red fluorescence signals with the corresponding increase in green fluorescence signals of JC-1 dye (Figure 9). As a positive control valinomycin, which is identified to depolarize mitochondria, was used, where only green signals of JC-1 dye was observed.⁵¹ The cells that were treated with complex **2** and set aside in dark displayed no apparent change in red and green signals in CLSM images recorded under similar experimental conditions.

CONCLUSIONS

In summary, platinum(II) complexes **1** and **2** of the red-light photosensitizer R-BODIPY were successfully developed as targeted near-IR red-light PDT agents. Complex **2** with an appended glucose moiety showed significantly high cellular uptake in cancer cells compared to complex **1**.²¹ The complexes showed higher cellular uptake in cancer cells than in normal cells. The R-BODIPY complexes displayed significant mitochondrial localization as evidenced from CLSM images, with moderately high Pearson's coefficient values (~ 0.7) for complex **2** and R-BODIPY. Both the complexes exhibited excellent PDT activity in near-IR red light with low IC_{50} values, while showing nominal dark toxicity. Their fluorescence property enabled us to image the platinum complexes for distribution in the living cells. The complexes belonging to the emerging class of photoactive monofunctional platinum(II) complexes showed red light induced release of the photoactive R-BODIPY ligand, which generates singlet oxygen with high quantum yield. The complexes satisfy all the major requirements of targeted PDT by showing low IC_{50} values in red light, high IC_{50} values in dark, singlet oxygen as the ROS, localizing in mitochondria over nucleus, and finally differential cellular uptake between normal versus cancer cells facilitated by a glucose moiety in the tpy ligand structure. The results are of significance toward developing complex **2** as a promising targeted PDT agent in near-IR red light.

ASSOCIATED CONTENT

Supporting Information

The Supporting Information is available free of charge on the ACS Publications website at DOI: 10.1021/acs.inorgchem.7b02249.

Reaction schemes, ESI-mass, ¹H NMR, and IR spectra, stability plot, unit cell packing, optimized structures, FMOs, MTT assay, cellular uptake, CV assay, ICP-MS, DCFDA assay, mass spectra of the photoirradiated complex **1**, confocal images, crystallographic details, bond distances/angles, and Cartesian coordinates of **1** and **2** (PDF)

Accession Codes

CCDC 1563252 contains the supplementary crystallographic data for this paper. These data can be obtained free of charge via www.ccdc.cam.ac.uk/data_request/cif, or by emailing data_request@ccdc.cam.ac.uk, or by contacting The Cambridge Crystallographic Data Centre, 12 Union Road, Cambridge CB2 1EZ, UK; fax: +44 1223 336033.

AUTHOR INFORMATION

Corresponding Authors

*E-mail: arc@iisc.ac.in. (A.R.C.)

*E-mail: paturu@iisc.ac.in. (P.K.)

ORCID

Vanitha Ramu: 0000-0003-4438-1071

Srishti Gautam: 0000-0002-6266-9709

Aditya Garai: 0000-0002-0972-5580

Paturu Kondaiah: 0000-0002-2159-1044

Akhil R. Chakravarty: 0000-0002-6471-9167

Notes

The authors declare no competing financial interest.

ACKNOWLEDGMENTS

A.R.C. thanks the Department of Science and Technology (DST), Government of India, for financial support (SR/SS/MBD-02/2007 and EMR/2015/000742) and for J. C. Bose national fellowship. P.K.'s research group is funded by DBT-IISc grants. V.R. thanks M. K. Raza for his help in the initial work. We are thankful to Urvashi for FACS data and to Saima and Divya for confocal microscopy images.

REFERENCES

- (1) Johnstone, T. C.; Suntharalingam, K.; Lippard, S. J. The Next Generation of Platinum Drugs: Targeted Pt(II) Agents, Nanoparticle Delivery and Pt(IV) Prodrugs. *Chem. Rev.* **2016**, *116*, 3436–3486.
- (2) Farrell, N. P. Multi-Platinum Anti-Cancer Agents. Substitution-Inert Compounds for Tumor Selectivity and New Targets. *Chem. Soc. Rev.* **2015**, *44*, 8773–8785.
- (3) Dhar, S.; Kolishetti, N.; Lippard, S. J.; Farokhzad, O. C. Targeted Delivery of a Cisplatin Prodrug for Safer and More Effective Prostate Cancer Therapy. *Proc. Natl. Acad. Sci. U. S. A.* **2011**, *108*, 1850–1855.
- (4) (a) Pizarro, A. M.; McQuitty, R. J.; Mackay, F. S.; Zhao, Y.; Woods, J. A.; Sadler, P. J. Cellular Accumulation, Lipophilicity and Photocytotoxicity of Diazo Platinum(IV) Anticancer Complexes. *ChemMedChem* **2014**, *9*, 1169–1175. (b) Mackay, F. S.; Woods, J. A.; Heringová, P.; Kaspárková, J.; Pizarro, A. M.; Moggach, S. A.; Parsons, S.; Brabec, V.; Sadler, P. J. A Potent Cytotoxic Photoactivated Platinum Complex. *Proc. Natl. Acad. Sci. U. S. A.* **2007**, *104*, 20743–20748.
- (5) (a) Schatzschneider, U. Photoactivated Biological Activity of Transition-Metal Complexes. *Eur. J. Inorg. Chem.* **2010**, 1451–1467. (b) Wickramasinghe, L. A.; Sharp, P. R. Photoreduction of Pt(IV) Halo-Hydroxo Complexes: Possible Hypohalous Acid Elimination. *Inorg. Chem.* **2014**, *53*, 1430–1442.
- (6) Farrer, N. J.; Salassa, L.; Sadler, P. J. Photoactivated Chemotherapy (PACT): The Potential of Excited-State d-block Metals in Medicine. *Dalton Trans.* **2009**, 10690–10701.
- (7) Castano, A. P.; Mroz, P.; Hamblin, M. R. Photodynamic Therapy and Anti-Tumor Immunity. *Nat. Rev. Cancer* **2006**, *6*, 535–545.
- (8) (a) Robertson, C. A.; Evans, D. H.; Abrahamse, H. Photodynamic Therapy (PDT): A Short Review on Cellular Mechanisms and Cancer Research Applications for PDT. *J. Photochem. Photobiol., B* **2009**, *96*, 1–8. (b) Mari, C.; Pierroz, V.; Ferrari, S.; Gasser, G. Combination of Ru(II) Complexes and Light: New Frontiers in Cancer Therapy. *Chem. Sci.* **2015**, *6*, 2660–2686.
- (9) (a) Wang, X.; Guo, Z. Targeting and Delivery of Platinum-Based Anticancer Drugs. *Chem. Soc. Rev.* **2013**, *42*, 202–224. (b) Lovell, J. F.; Liu, T. W. B.; Chen, J.; Zheng, G. Activable Photosensitizers for Imaging and Therapy. *Chem. Rev.* **2010**, *110*, 2839–2857.
- (10) Raza, M. K.; Mitra, K.; Shettar, A.; Basu, U.; Kondaiah, P.; Chakravarty, A. R. Photoactive Platinum(II) β -diketonates as Dual Action Anticancer Agents. *Dalton Trans.* **2016**, *45*, 13234–13243.
- (11) Miller, M. A.; Zheng, Y. R.; Gadde, S.; Pfirschke, C.; Zope, H.; Engblom, C.; Kohler, R. H.; Iwamoto, Y.; Yang, K. S.; Askevold, B.;

- Kolishetti, N.; Pittet, M.; Lippard, S. J.; Farokhzad, O. C.; Weissleder, R. Tumour-Associated Macrophages Act as a Slow-release Reservoir of Nanotherapeutic Pt(IV) Pro-drug. *Nat. Commun.* **2015**, *6*, 8692–8704.
- (12) Miller, M. A.; Askevold, B.; Yang, K. S.; Kohler, R. H.; Weissleder, R. Platinum Compounds for High-Resolution in Vivo Cancer Imaging. *ChemMedChem* **2014**, *9*, 1131–1135.
- (13) Guo, Z.; Zou, Y.; He, H.; Rao, J.; Ji, S.; Cui, X.; Ke, H.; Deng, Y.; Yang, H.; Chen, C.; Zhao, Y.; Chen, H. Bifunctional Platinated Nanoparticles for Photoinduced Tumor Ablation. *Adv. Mater.* **2016**, *28*, 10155–10164.
- (14) Pansare, V.; Hejazi, S.; Faenza, W.; Prud'homme, R. K. Review of Long-Wavelength Optical and NIR Imaging Materials: Contrast Agents, Fluorophores and Multifunctional Nano Carriers. *Chem. Mater.* **2012**, *24*, 812–827.
- (15) Mao, J.; Zhang, Y.; Zhu, J.; Zhang, C.; Guo, Z. Molecular Combo of Photodynamic Therapeutic Agent Silicon(IV) Phthalocyanine and Anticancer Drug Cisplatin. *Chem. Commun.* **2009**, 908–910.
- (16) Liu, Y.; Li, Z.; Chen, L.; Xie, Z. Near Infrared BODIPY-Platinum Conjugates for Imaging, Photodynamic Therapy and Chemotherapy. *Dyes Pigm.* **2017**, *141*, 5–12.
- (17) Srinivasarao, M.; Galliford, C. V.; Low, P. S. Principles in the Design of Ligand-Targeted Cancer Therapeutics and Imaging Agents. *Nat. Rev. Drug Discovery* **2015**, *14*, 203–219.
- (18) Patra, M.; Awuah, S. G.; Lippard, S. J. Chemical Approach to Positional Isomers of Glucose-Platinum Conjugates Reveals Specific Cancer Targeting through Glucose-Transporter-Mediated Uptake in Vitro and in Vivo. *J. Am. Chem. Soc.* **2016**, *138*, 12541–12551.
- (19) Mjos, K. D.; Orvig, C. Metallo drugs in Medicinal Inorganic Chemistry. *Chem. Rev.* **2014**, *114*, 4540–4563.
- (20) Macheda, M. L.; Rogers, S.; Best, J. D. Molecular and Cellular Regulation of Glucose Transporter (GLUT) Proteins in Cancer. *J. Cell. Physiol.* **2005**, *202*, 654–662.
- (21) Basu, U.; Khan, I.; Hussain, A.; Gole, B.; Kondaiah, P.; Chakravarty, A. R. Carbohydrate-Appended Tumor Targeting Iron(III) Complexes Showing Photocytotoxicity in Red Light. *Inorg. Chem.* **2014**, *53*, 2152–2162.
- (22) Frantz, M. C.; Wipf, P. Mitochondria as a Target in Treatment. *Environ. Mol. Mutagen.* **2010**, *51*, 462–475.
- (23) (a) Chatterjee, A.; Mambo, E.; Sidransky, D. Mitochondrial DNA Mutations in Human Cancer. *Oncogene* **2006**, *25*, 4663–4674. (b) Sun, T.; Guan, X.; Zheng, M.; Jing, X.; Xie, Z. Mitochondria-Localized Fluorescent BODIPY-Platinum Conjugate. *ACS Med. Chem. Lett.* **2015**, *6*, 430–433.
- (24) Pereira, N. A.; Laranjo, M.; Casalta-Lopes, J.; Serra, A. C.; Pineiro, M.; Pina, J.; Seixas de Melo, J. S.; Senge, M. O.; Botelho, M. F.; Martelo, L.; Burrows, H. D.; Pinho e Melo, T. M. V. D. Platinum(II) Ring-Fused Chlorins as Near-Infrared Emitting Oxygen Sensors and Photodynamic Agents. *ACS Med. Chem. Lett.* **2017**, *8*, 310–315.
- (25) Xue, X.; Zhu, C.; Chen, H.; Bai, Y.; Shi, X.; Jiao, Y.; Chen, Z.; Miao, Y.; He, W.; Guo, Z. A New Approach to Sensitize Antitumor Monofunctional Platinum(II) Complexes via Short Time Photo-Irradiation. *Inorg. Chem.* **2017**, *56*, 3754–3762.
- (26) Mitra, K.; Gautam, S.; Kondaiah, P.; Chakravarty, A. R. The Cis-Diammineplatinum(II) Complex of Curcumin: A Dual Action DNA Crosslinking and Photochemotherapeutic Agent. *Angew. Chem., Int. Ed.* **2015**, *54*, 13989–13993.
- (27) Garai, A.; Pant, I.; Banerjee, S.; Banik, B.; Kondaiah, P.; Chakravarty, A. R. Photorelease and Cellular Delivery of Mitocurcumin from Its Cytotoxic Cobalt(III) Complex in Visible Light. *Inorg. Chem.* **2016**, *55*, 6027–6035.
- (28) Kamkaew, A.; Lim, S. H.; Lee, H. B.; Kiew, L. V.; Chung, L. Y.; Burgess, K. BODIPY Dyes in Photodynamic Therapy. *Chem. Soc. Rev.* **2013**, *42*, 77–88.
- (29) Ni, Y.; Wu, J. Far-red and Near Infrared BODIPY Dyes: Synthesis and Applications for Fluorescent pH Probes and Bio-imaging. *Org. Biomol. Chem.* **2014**, *12*, 3774–3791.
- (30) Raza, M. K.; Mitra, K.; Gautam, S.; Garai, A.; Kondaiah, P.; Chakravarty, A. R. Monofunctional BODIPY-Appended Imidazopylatin for Cellular Imaging and Mitochondria-Targeted Photocytotoxicity. *Inorg. Chem.* **2017**, *56*, 11019–11029.
- (31) Mitra, K.; Gautam, S.; Kondaiah, P.; Chakravarty, A. R. BODIPY-Appended 2-(2-Pyridyl)benzimidazole Platinum(II) Catecholates for Mitochondria-Targeted Photocytotoxicity. *ChemMedChem* **2016**, *11*, 1956–1967.
- (32) (a) Arena, G.; Scolaro, L. M.; Pasternack, R. F.; Romeo, R. Synthesis, Characterization, and Interaction with DNA of the Novel Metallointercalator Cationic Complex (2,2':6',2''-Terpyridine)-methylplatinum(II). *Inorg. Chem.* **1995**, *34*, 2994–3002. (b) Mitra, K.; Basu, U.; Khan, I.; Maity, B.; Kondaiah, P.; Chakravarty, A. R. Remarkable Anticancer Activity of Ferrocenylterpyridine Platinum(II) Complexes in Visible Light with Low Dark Toxicity. *Dalton Trans.* **2014**, 43, 751–763.
- (33) Godoy, J.; Vives, G.; Tour, J. M. Synthesis of Highly Fluorescent BODIPY-Based Nanocars. *Org. Lett.* **2010**, *12*, 1464–1467.
- (34) Jia, H.; Küçüköz, B.; Xing, Y.; Majumdar, P.; Zhang, C.; Karatay, A.; Yaglioglu, G.; Elmali, A.; Zhao, J.; Hayvali, M. *trans*-Bis-(alkylphosphine) Platinum(II)-Alkynyl Complexes Showing Broad-band Visible Light Absorption and Long-lived Triplet Excited States. *J. Mater. Chem. C* **2014**, *2*, 9720–9736.
- (35) Frisch, M. J.; et al. *Gaussian 09*, Revision D.01; Gaussian, Inc.: Wallingford, CT, 2009 (see Supporting Information ref 4 for full citation).
- (36) Nastasi, F.; Puntoriero, F.; Campagna, S.; Olivier, J. H.; Ziessel, R. Hybrid complexes: Pt(II)-terpyridine linked to various acetylidobipyridyl subunits. *Phys. Chem. Chem. Phys.* **2010**, *12*, 7392–7402.
- (37) Mitra, K.; Shettar, A.; Kondaiah, P.; Chakravarty, A. R. Biotinylated Platinum(II) Ferrocenylterpyridine Complexes for Targeted Photoinduced Cytotoxicity. *Inorg. Chem.* **2016**, *55*, 5612–5622.
- (38) Zhao, T.; Liu, R.; Shi, H.; Shu, M.; Hu, J.; Li, H.; Zhu, H. Synthesis, Tunable Photophysics and Nonlinear Absorption of Terpyridyl Pt(II) Complexes Bearing Different Acetylidyl Ligands. *Dyes Pigm.* **2016**, *126*, 165–172.
- (39) (a) Sheldrick, G. M. Crystal Structure Refinement with SHELXL. *Acta Crystallogr., Sect. C: Struct. Chem.* **2015**, *71*, 3–8. (b) Farrugia, L. J. WinGX and ORTEP for Windows: an update. *J. Appl. Crystallogr.* **2012**, *45*, 849–854. (c) Walker, N.; Stuart, D. An Empirical Method for Correcting Diffractometer Data for Absorption Effects. *Acta Crystallogr., Sect. A: Found. Crystallogr.* **1983**, *39*, 158–166.
- (40) Skehan, P.; Storeng, R.; Scudiero, D.; Monks, A.; McMahon, J.; Vistica, D.; Warren, J. T.; Bokesch, H.; Kenney, S.; Boyd, M. R. New Colorimetric Cytotoxicity Assay for Anticancer-Drug Screening. *J. Natl. Cancer Inst.* **1990**, *82*, 1107–1112.
- (41) (a) Barron, C.; Tsiani, E.; Tsakiridis, T. Expression of the glucose transporters GLUT1, GLUT3, GLUT4 and GLUT12 in human cancer cells. *BMC Proc.* **2012**, *6*, P4. (b) Rodríguez-Enríquez, S.; Marín-Hernández, A.; Gallardo-Pérez, J. C.; Moreno-Sánchez, R. Kinetics of Transport and Phosphorylation of Glucose in Cancer Cells. *J. Cell. Physiol.* **2009**, *221*, 552.
- (42) Chung, C. Y. S.; Li, S. P. Y.; Lo, K. K. W.; Yam, V. W. W. Synthesis and Electrochemical, Photophysical, and Self-Assembly Studies on Water-Soluble pH-Responsive Alkynylplatinum(II) Terpyridine Complexes. *Inorg. Chem.* **2016**, *55*, 4650–4663.
- (43) (a) Diring, S.; Puntoriero, F.; Nastasi, F.; Campagna, S.; Ziessel, R. Star-Shaped Multichromophoric Arrays from Bodipy Dyes Grafted on Truxene Core. *J. Am. Chem. Soc.* **2009**, *131*, 6108–6110. (b) Ziessel, R.; Ulrich, G.; Elliott, K. J.; Harriman, A. Electronic Energy Transfer in Molecular Dyads Built Around Boron-Ethyne-Substituted Subphthalocyanines. *Chem. - Eur. J.* **2009**, *15*, 4980–4984.
- (44) (a) Geist, F.; Jackel, A.; Irmeler, P.; Linseis, M.; Malzkuhn, S.; Kuss-Petermann, M.; Wenger, O. S.; Winter, R. F. Directing Energy Transfer in Panchromatic Platinum Complexes for Dual Vis–Near-IR or Dual Visible Emission from σ -Bonded BODIPY Dyes. *Inorg. Chem.* **2017**, *56*, 914–930. (b) Yu-Tzu Li, E.; Jiang, T.-Y.; Chi, Y.; Chou, P.-T. Semi-quantitative Assessment of the Intersystem Crossing Rate: an

Extension of the El-Sayed Rule to the Emissive Transition Metal Complexes. *Phys. Chem. Chem. Phys.* **2014**, *16*, 26184–26192.

(45) Ziessel, R.; Ulrich, G.; Harriman, A.; Alamiry, M. A. H.; Stewart, B.; Retailleau, P. Solid-State Gas Sensors Developed from Functional Difluoroboradiazaindacene Dyes. *Chem. - Eur. J.* **2009**, *15*, 1359–1369.

(46) Sliwka, L.; Wiktorska, K.; Suchocki, P.; Milczarek, M.; Mielczarek, S.; Lubelska, K.; Cierpial, T.; Lyzwa, P.; Kielbasinski, P.; Jaromin, A.; Flis, A.; Chilmonczyk, Z. The Comparison of MTT and CVS Assays for the Assessment of Anticancer Agent Interactions. *PLoS One* **2016**, *11*, e0155772.

(47) Patra, M.; Johnstone, T. C.; Suntharalingam, K.; Lippard, S. J. A Potent Glucose-Platinum Conjugate Exploits Glucose Transporters and Preferentially Accumulates in Cancer Cells. *Angew. Chem., Int. Ed.* **2016**, *55*, 2550–2554.

(48) (a) Gandra, N.; Frank, A. T.; Le Gendre, O.; Sawwan, N.; Aebisher, D.; Liebman, J. F.; Houk, K. N.; Greer, A.; Gao, R. Possible Singlet Oxygen generation from the Photolysis of Indigo dyes in Methanol, DMSO, Water and Ionic liquid, 1-butyl-3-methylimidazolium tetrafluoroborate. *Tetrahedron* **2006**, *62*, 10771–10776. (b) Marques-Santos, L. F.; Coqueiro, V. M.; Rumjanek, V. M. Cyclosporin A Does Not Protect the Disruption of the Inner Mitochondrial Membrane Potential Induced by Potassium Ionophores in Intact K562 cells. *Cell Boil. Int.* **2006**, *30*, 197–204. (c) Adarsh, N.; Shanmugasundaram, M.; Avirah, R. R.; Ramaiah, D. Aza-BODIPY Derivatives: Enhanced Quantum Yields of Triplet Excited States and the Generation of Singlet Oxygen and their Role as Facile Sustainable Photooxygenation Catalysts. *Chem. - Eur. J.* **2012**, *18*, 12655–12662.

(49) Wang, P.; Koo, Y. H.; Kim, W.; Yang, W.; Cui, X.; Ji, W.; Zhao, J.; Kim, D. Broadband Visible Light Harvesting N^N Pt(II) Bisacetylde Complex with Bodipy and Naphthalene Diimide Ligands: Förster Resonance Energy Transfer and Intersystem Crossing. *J. Phys. Chem. C* **2017**, *121*, 11117–11128.

(50) Dunn, K. W.; Kamocka, M. M.; McDonald, J. H. A Practical Guide to Evaluating Colocalization in Biological Microscopy. *Am. J. Physiol. Cell. Physiol.* **2011**, *300*, C723–C742.

(51) Felber, S. M.; Brand, M. D. Valinomycin Can Depolarize Mitochondria in Intact Lymphocytes Without Increasing Plasma Membrane Potassium Fluxes. *FEBS Lett.* **1982**, *150*, 122–124.